IEEE Photonics Journal
An IEEE Photonics Society Publication

A New Method for Determining the Sampling Volume and the Number of Particles Within It for Particle Concentration Identification in Defocused Interferometric Particle Imaging

Volume 9, Number 1, February 2017

Hongxia Zhang
Ye Zhou
Jing Liu
Dagong Jia
Tiegen Liu

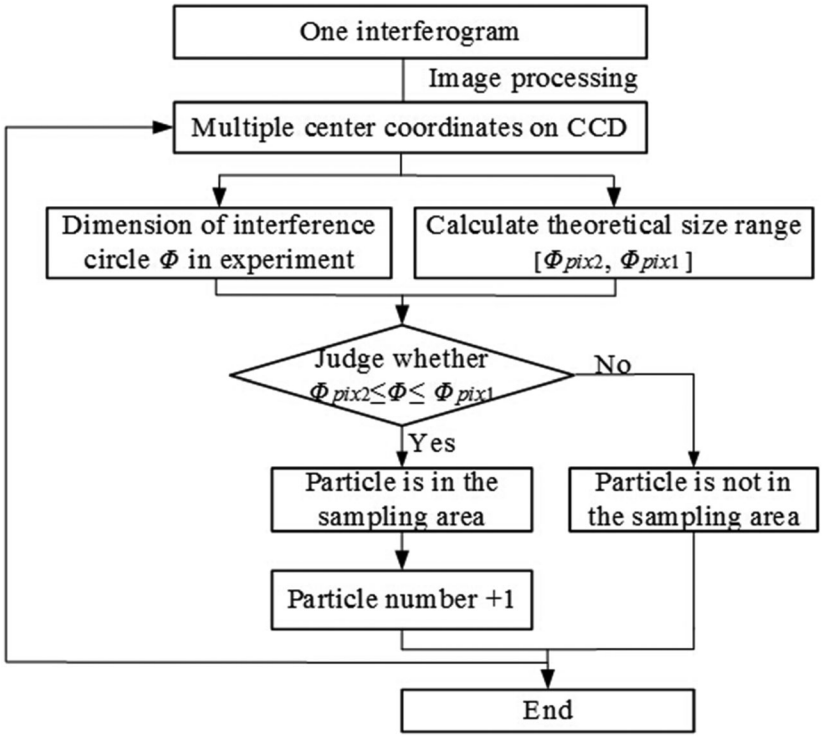

DOI: 10.1109/JPHOT.2017.2648258
1943-0655 © 2017 IEEE

A New Method for Determining the Sampling Volume and the Number of Particles Within It for Particle Concentration Identification in Defocused Interferometric Particle Imaging

Hongxia Zhang,[1,2] Ye Zhou,[1,2] Jing Liu,[1,2] Dagong Jia,[1,2] and Tiegen Liu[1,2]

[1]College of Precision Instrument and Optoelectronics Engineering, Tianjin University, Tianjin 300072, China
[2]Key Laboratory of Optoelectronics Information Technical Science, EMC, Tianjin 300072, China

DOI:10.1109/JPHOT.2017.2648258

Manuscript received November 28, 2016; revised December 27, 2016; accepted December 31, 2016. Date of publication January 9, 2017; date of current version January 25, 2017. This work was supported by the National Natural Sciences Foundation under Grant 41275146. Corresponding author: Hongxia Zhang (e-mail: hxzhang@tju.edu.cn).

Abstract: Interferometric particle imaging (IPI) is a robust technique for measuring particle size and velocity. In defocused IPI that is uniquely valuable to quality control of a spray field, a reliable method for identifying the particle concentration in the volume sampled by the sheet beam remains outstanding. This paper proposes a new approach to the determination of the sampling volume of defocused IPI and the number of particles within the sampling volume for informing the particle concentration. The methods for determining the sampling volume and the number of particles within the sampling volume are documented with a new set of formula derived using conventional ray-tracing and interferometry principles. For any defined measurement geometry, the sampling volume is quantitated when the lateral and elevational dimensions of the sheet beam and the defocusing distance are known. The number of particles in the sampling volume is counted by determining whether or not a particle is within the sampling volume, upon the analysis of the size range $[\Phi_{pix2}, \Phi_{pix1}]$ of the interference circle. The method for identifying particle concentration in defocused IPI is tested on synthetic interferogram (1% noise) corresponding to first, particles of the same size of 45 μm at different concentrations ranging from 0.0040 to 0.239 mm^{-3} and, second, particles of 0.0119 and 0.119 mm^{-3} concentrations with the sizes ranging from 10 to 90 μm. This new method for quantitating particle concentration in defocused IPI is then examined against experimental concentrations of particles of 10, 21.3, and 45 μm in size, respectively. The largest experimental error for 45 μm particles with the concentration of 0.006 mm^{-3} is 10.4% and decreases with the increase of the particle concentration. This method for identifying particle concentration is expected to be applicable to various areas wherein particle analysis is to be rendered by defocused IPI.

Index Terms: Interferometric particle imaging (IPI), particle concentration, sampling volume, particle identification.

1. Introduction

Interferometric particle imaging (IPI) originally proposed by König [1] in 1986 is a technique for acquiring the particle information. It has become a popular and effective modality for measuring the size and velocity of various particles [2]–[5]. In 2000, Niwa [6] realized measurement of the velocity of the transparent spherical bubble by tracking the movement and continuously acquiring the image sequence, while obtaining the diameter of the bubble by counting the number of fringes or fringe spacing. In 2005, Zama [7] combined in-focus and out-of-focus IPI to simultaneously determine of the size and velocity of droplets. The size was evaluated by the glare-point separation and the fringe order of the interferogram and the velocity were obtained by 3D Particle Image Velocimetry (PIV). Besides the studies that chronicled the advancement of measurement devices, a number of works have focused on methods, both hardware-enabled or algorithm-based, that enhance the accuracy and speed of particle identification as well as the robustness of identifying particles of different shapes. In 2009, A Querel *et al.* [8] accelerated the speed of image processing by applying a one-dimensional Fourier transform for identifying droplets of diameters between 20 and 250 μm, which accelerated the processing 20 times and reached an end-image formation speed of 0.7 s per image on Pentium Xenon at 2 GHz. In 2012, Shen *et al.* [9] traced the position of spherical particles by using a cylindrical lens in the Interferometric out-of-focus Imaging. The longitudinal position was determined through the fringe's orientation, and the transverse position was given by the image's location on CCD. Shen *et al.* also deduced the diameter from the frequency of the fringes. In 2014, Brunel *et al.* [10] presented an analytical method that predicted speckle-like interferometric out-of-focus patterns created by irregular scattering objects in typical IPI system. Brunel *et al.* used the central peak of the 2-D-autocorrelation patterns to recover the particle dimensions. In 2014, Carrascal *et al.* [11] proposed a sizing algorithm in IPI system based on detecting the maximum curvature of the peak corresponding to the Fourier transform of the speckle pattern of sand particles when in or not in motion. In that study, the image blurring often associated with the use of a continuous wave laser in IPI was carefully mitigated by controlling the exposure time.

There has been abundance of technologies in regard to IPI based determination of particle size and velocity. Yet, there is a limited number of IPI methods that can robustly inform particle concentration, a parameter that is of specific importance to applications including quality control of spray field. In 2000, Maeda [12] measured the size and velocity of particles with high concentration by adding a pair of cylindrical lens to IPI system to transform the circular interferograms into the linear interferograms; in 2002, Damaschke [13] studied the relation of the maximal measurable particle concentration with the IPI system parameters including the object distance, the thickness of the sheet beam, and the aperture and focal length of the imaging lens. In 2015, Evans *et al.* [14] demonstrated a novel algorithm that obtained the particle size probability density from IPI data. That approach can be extended to analyzing the overlapped particle images. In 2011, Yi Wang *et al.* [15] presented a statistic method for identifying the concentration of particles in flow based on optical coherence tomography (OCT). Wang's method was based on the principle that the fluctuating numbers of particles contained within a small OCT detection volume caused by Brownian motion are governed by Poisson distribution. In 2012, S. Buaprathooma *et al.* [16] proposed a system with multiple-angle detections and used Partial Least Square Regression (PLS-R) to reconstruct the scattering angles for particle concentration identification. Thus far, however, there is no report on the use of defocused IPI for measuring the particle concentration.

To the author's knowledge, particle concentration identification based on defocused IPI has not been reported. Several studies based on IPI system have focused on identifying the size and velocity of the particles, whereas an efficient and accurate method for identifying sampling volume has remained to be developed accurately. Conventionally the particles within in a sampling volume is judged by deriving the three-dimensional coordinates of each particle, enabling the subsequent counting of particle number and concentration that are time consuming. This paper proposes a new method for determining the sampling volume and the number of particles within it for particle concentration identification in defocused IPI. As IPI operates upon an oblique object plane, the volume of particle interrogated by the sampling beam in IPI differs from that of conventional imaging

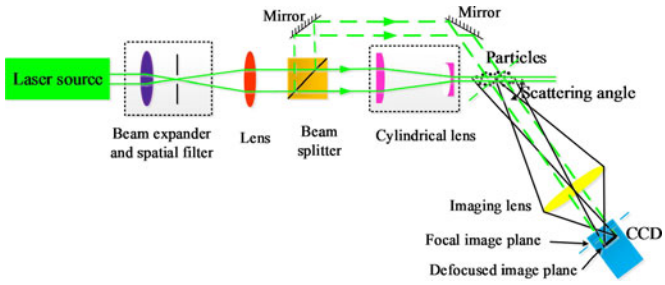

Fig. 1. Schematic diagram of defocused IPI for modeling the sample volume.

systems operating on object planes that are usually normal to the optical axis. For the calculation of the sampling volume of IPI, a method of quantifying the sampling volume of focused IPI which is based on the geometrical optics was presented by Zhang *et al.* [17] in 2015. The new method proposed in this article quantifies the sampling volume of defocused IPI based on the ray-tracing and interferometry principle. Furthermore, the sampling volume at the object space can be directly obtained by deducing to the corresponding size range of the particle interference circle at the image plane. Then, by judging the size of interference circle formed by the particle, whether or not the particle is in the sampling volume is determined. Accordingly, the particle number and concentration can be derived. In addition, the simulations of particles with different sizes and concentrations are applied to validate the algorithm. Finally, the method was examined experimentlly with a defocused IPI system and the particles with various sizes and concentrations are also conducted.

2. Theory

The schematic diagram as shown in Fig. 1 is used for modeling of the sampling volume in a typical configuration of defocused IPI. A laser beam passes a beam expander and a spatial filter that rejects the stray light, and then passes a lens to become a collimated light beam. The beam is then divided into two beams by a beam splitter. One beam (the solid line passing the beam splitter) is shaped by two cylindrical lenses to a sheet beam for interrogating the sample of particles. The other beam (the dashed line reflected by the beam splitter) is directed to the imaging lens and a CCD camera by two mirrors. This second beam forms an auxiliary light path for adjusting the optical path and it is blocked during the experiment. When the sheet beam illuminates the particles, it would be reflected by the particle surface and refracted once in the particle. The refracted light exits from the interior of the particle and two beams would interfere with each other, thus forming two-point images at the focal image plane and fringe patterns at the defocused image plane. Both the two-point images and the fringe patterns are acquired by the same CCD camera. As is shown in Fig. 1, the beam plane in this defocused IPI is also the object plane and at an oblique angle with respect to the image plane. The particles that will form an image on the CCD camera are those confined in the sampling volume that is determined by the thickness of the sheet beam and the geometry of the imaging lens and the CCD.

2.1 Ray-Tracing Based Characterization of the Sampling Volume

Fig. 2 details the ray-tracing geometry defining an object-image relation in a defocused IPI where the sampling volume to be modeled is marked by the shadowed area at the left. In Fig. 2, OP denotes the object plane, LP the imaging lens plane, and IP the CCD image plane. IP is in parallel with LP, but not with OP. Z_R is the distance between LP and IP. θ is the angle of scattering that is also the angle between the sheet beam and the optical axis of imaging lens. t is the thickness of the sheet beam. The points O_1', O_2', O_3' are respectively the images of the points of O, O_1, and O_2, and A′, A_1', and A_2' are, respectively, the images of the points A, A_1, and A_2. g_* is correspondingly

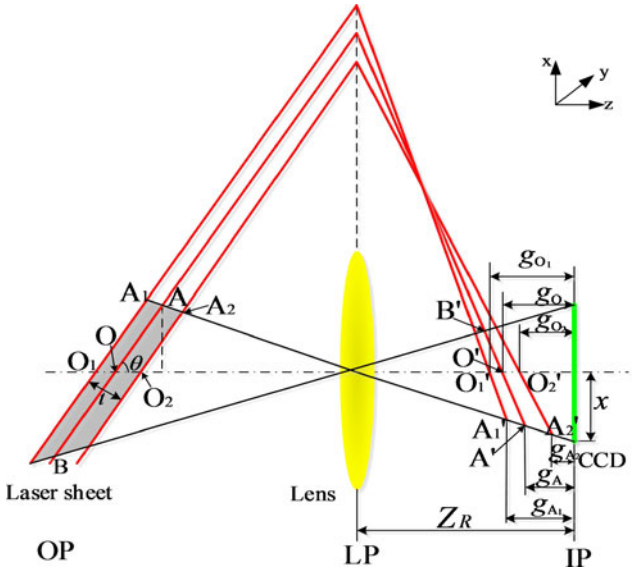

Fig. 2. Ray-tracing geometry determining the object-image relation in a defocused IPI.

the defocused displacement (for instance, g_o is the defocused displacement of the central point O). x represents the lateral displacement of a point with respect to the central line of CCD.

The maximum sampling volume is obtained when the image points A' and B' locate at the edge of the CCD, which will give $x = a/2$, where a is the lateral dimension of the CCD at the plane of interest. The object distances of points A and B are then

$$u_A = \frac{(u_o - l/\sin\theta)\cdot\tan\theta}{\tan\theta + a/(2Z_R)} \tag{1}$$

$$u_B = \frac{(u_o - l/\sin\theta)\cdot\tan\theta}{\tan\theta - a/(2Z_R)} \tag{2}$$

where l is the distance of the object plane from the central plane of the sheet beam.

In the trapezoid representing the sampling volume, the lengths h_{-A} and h_{-B} of the two sides that pass respectively the points A and B on OP are

$$h_{-A} = b\cdot u_A/Z_R \tag{3}$$

$$h_{-B} = b\cdot u_B/Z_R \tag{4}$$

where b is the height of the CCD. The distance between point A and B is

$$\overline{AB} = (u_B - u_A)/\cos\theta. \tag{5}$$

The projection of the trapezoidal sampling volume onto the CCD image plane is illustrated in Fig. 3 which shows how the imaging area of the trapezoid is related to the height of the sheet beam h_{st}. Three conditions of the sheet beam height are represented in Fig. 1: 1) for the beam being wider than h_{-B} 2) for the beam being narrower than h_{-B} but wider than h_{-A} 3) for the beam being narrower than h_{-A}. The object area at each of the three beam sizes can be calculated as the following:

1) If $h_{st} > h_{-B}$ as is shown by Fig. 3(a), the entire trapezoidal plane will be imaged on to the CCD, and the area of the trapezoid is then

$$S = \frac{1}{2}(h_{-A} + h_{-B})\cdot\overline{AB}. \tag{6}$$

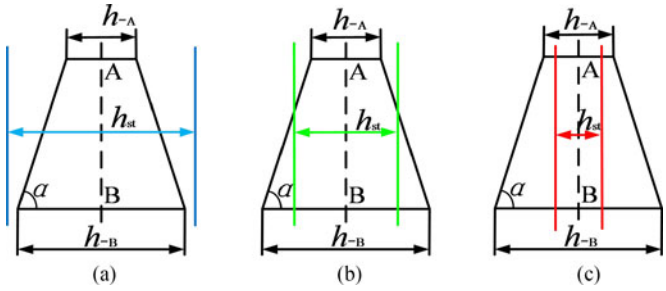

Fig. 3. Trapezoid at object space.

2) If $h_{-A} < h_{st} < h_{-B}$ as is shown by Fig. 3(b), the object plane that will be imaged on to the CCD is a hexagon, with an area of

$$S = \frac{1}{2}(h_{-A} + h_{-B}) \cdot \overline{AB} - \frac{1}{4}(h_{-B} - h_{st})^2 \cdot \tan\alpha. \tag{7}$$

3) If $h_{st} < h_{-A}$ as is shown by Fig. 3(c), the object plane that will be imaged on to the CCD is a rectangle, with an area of

$$S = h_{st} \cdot \overline{AB} \tag{8}$$

where h_{st} is also the diameter of the circular light beam at the light path prior to the cylindrical lens, and α is the base angle of the trapezoid. Regardless of the shape of the imaging area, the sampling volume can be expressed as

$$V = \int_{-t/2}^{t/2} Sdl. \tag{9}$$

2.2. Algorithm for Identifying the Particles Within the Sampling Volume

In defocused IPI system, the sampling volume at the object space can be derectly obtained based on the geometrical optics by deducing to the corresponding size range of the particle interference circle at the image plane. Then whether the particle is in the sampled volume can be determined by obtaining the dimension of interference circle of the particle. This method of identification is detailed in the following.

When points A_1 and A_2 are at the two edges of the sheet beam as is shown in Fig. 2, the maximal and minimal dimensions of the interference circles can be obtained. The first step of obtainging these two dimensions is to find the coordinates of A_1 and A_2 according to the coordinates of the interference circle. Then, the object distance of point A_2 is obtained by using the similarity of triangles as

$$u_{A_2} = \frac{\left(u_o - \frac{t}{2\cdot\sin\theta}\right) \cdot \tan\theta}{\tan\theta + x/Z_R}. \tag{10}$$

The image distance of point A_2, is then derived according to the object-image relationship as

$$v_{A_2} = \frac{f \cdot u_{A_2}}{u_{A_2} - f} \tag{11}$$

and the defocusing distance of point A_2 is given as

$$g_{A_2} = Z_R - v_{A_2}. \tag{12}$$

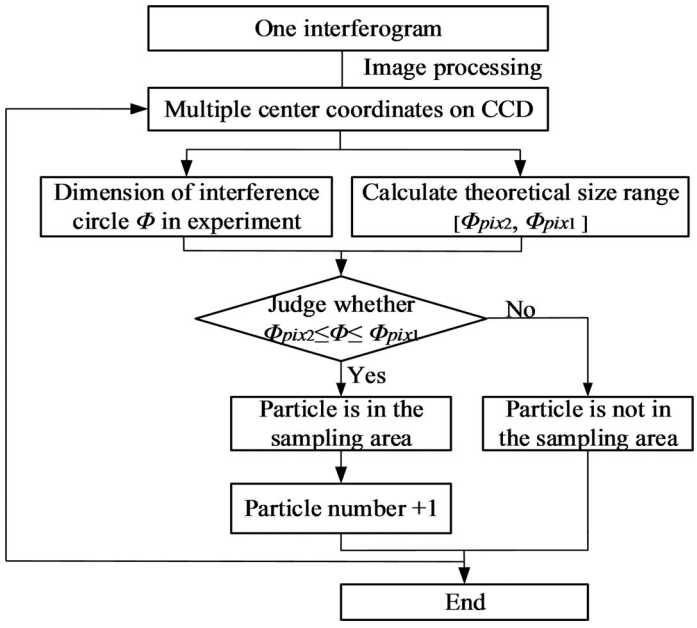

Fig. 4. Flow chart used for identifying the number of particles in the sampled volume.

The next step of obtaining the minimal and maximal dimensions of the interference circles is to determine the size Φ of the circle acquired by the CCD. It is formed with

$$\Phi = \frac{g \cdot d_a}{v \cdot \Delta x} \tag{13}$$

where d_a is the clear aperture of imaging lens, and Δx is one pixel size.

Thus, the size of the circle formed by the particle at point A_2 is given as

$$\Phi_{pix2} = \frac{g_{A_2} \cdot d_a}{v_{A_2} \cdot \Delta x}. \tag{14}$$

The size of the circle formed by the particle at point A_1 can be obtained similarly, by using object distance u_{A_1}, image distance v_{A_1}, magnification β_{A_1}, and defocusing distance g_{A_1}. The resulted Φ_{pix1} of the circle is

$$\Phi_{pix1} = \frac{g_{A_1} \cdot d_a}{v_{A_1} \cdot \Delta x}. \tag{15}$$

The image points A_1' and A_2' are at the same position on the CCD, so the size of the circle is to be determined by the defocusing distance g and the image distance v. According to the geometrical relation shown in Fig. 2, the size range of interference circles at every position on CCD is expressed as $[\Phi_{pix2}, \Phi_{pix1}]$. When the thickness of the sheet beam is a constant value and the size Φ of the interference circle is obtained, whether or not this particle is in the sampling volume will be determined by the size range. The algorithm for identifying the number of particles in the sampled volume is outlined by the flow chart in Fig. 4.

According to the Fig. 4, the interferogram undergoes the image processing for extracting the coordinates of the particles. The extracted coordinates lead to the calculation of the size range $[\Phi_{pix2}, \Phi_{pix1}]$ and the size Φ. Whether the particle is in the sampled volume is then gauged by comparing the three dimensional parameters, specifically, the particle is in the sampling volume only if $\Phi_{pix2} \leq \Phi \leq \Phi_{pix1}$. After identifying all particles that are in the sampled volume, the number of the particles is obtained, as well as the particle concentration.

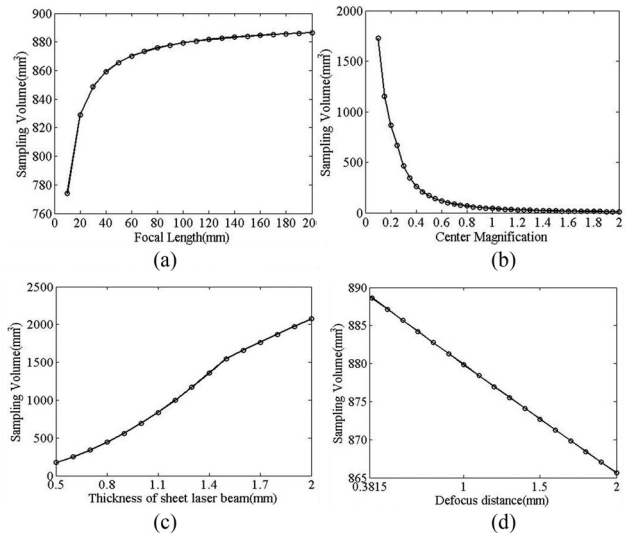

Fig. 5. Sampling volume with parameters of focal length, central magnification, thickness of sheet beam, and defocusing distance. (a) $\theta = 60^\circ$, $\beta_o = 0.2$, $p = 1$ mm, $g = 2$ mm. (b) $\theta = 60^\circ$, $f = 50$ mm, $p = 1$ mm, $g = 2$ mm. (c) $f = 50$ mm, $\theta = 60^\circ$, $\beta_o = 0.2$, $g = 2$ mm. (d) $f = 50$ mm, $\theta = 60^\circ$, $\beta_o = 0.2$, $p = 1$ mm.

3. Synthetic

3.1 Sampling Volume as Numerated by the Theory

According to above analyses, it can be known that the sampling volume is related to the focal length, center magnification, thickness of sheet beam and defocusing distance. Synthetic data representing the sampling volume are generated by various combinations of these parameters.

The sampling volume with varying parameters including focal length f, central magnification β_o, thickness of sheet beam p and defocusing distance g are simulated, as illustrated in Fig. 5. Fig. 5(a) shows the changing curve of the sampling volume with the focal length f of the imaging lens. The sampling volume increases as the focal length increases. When $f < 60$, the sampling volume increases quickly, and when $f > 60$, the sampling volume increases slowly. Fig. 5(b) shows the changing curve of the sampling volume with the central magnification. The sampling volume decreases as the central magnification increases. When $\beta_o < 0.6$, the sampling volume decreases fast, and when $\beta_o > 0.6$, the sampling volume stays almost unchangeable. Fig. 5(c) shows the changing curve of the sampling volume with the thickness of the sheet beam. The thicker the sheet beam, the bigger the sampling volume. Fig. 5(d) shows the changing curve of the sampling volume with the defocusing distance. The sampling volume decreases as the defocusing distance increases.

When the parameters including focal length and F-number of imaging lens, central magnification, the thickness of sheet beam, scattering angle, the defocusing distance, and the dimension of CCD target surface $a \times b$ are known, the sampling volume can be successfully calculated according to (1)–(9).

3.2 Performance of the Algorithm on the Synthetic Data

The system parameters are set as: $\beta_o = 0.20$, $u_o = 300.4$ mm, $v_o = 60$ mm and $g = 1.68$ mm. These parameters and experimental parameters for 45 μm particles are the same. Based on these parameters, according to (1)–(9) in the paper, the sampling volume can be calculated as 251.14 mm^3. The interferograms of particles with different concentrations or sizes have been simulated. The simulation results are shown as the followings.

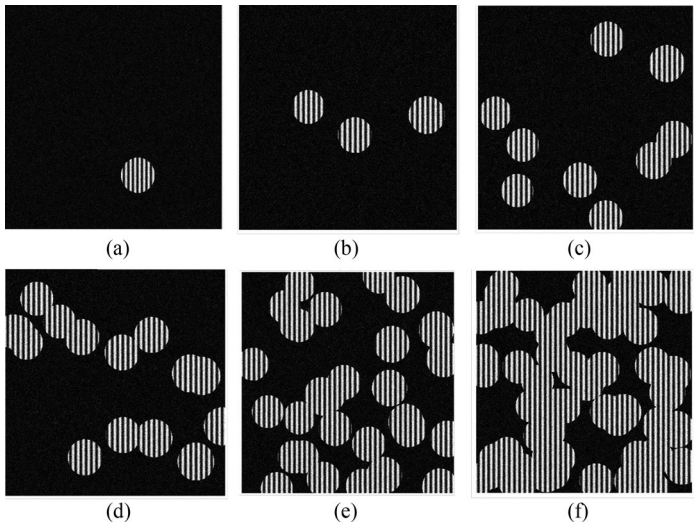

Fig. 6. Simulated interferograms of 45 μm particles under the white Gaussian noise with variance of 0.01. (a) $C = 0.0040\,\text{mm}^{-3}$. (b) $C = 0.0119\,\text{mm}^{-3}$. (c) $C = 0.0358\,\text{mm}^{-3}$. (d) $C = 0.0597\,\text{mm}^{-3}$. (e) $C = 0.119\,\text{mm}^{-3}$. (f) $C = 0.239\,\text{mm}^{-3}$.

The simulation results of the images of 45 μm particles with different concentrations are shown in Fig. 6. In all simulated images, a 1% white Gaussian noise to the light intensity is added. Fig. 6(a)–(f) respectively corresponds to a concentration of respectively 0.0040 mm^{-3}, 0.0119 mm^{-3}, 0.0358 mm^{-3}, 0.0597 mm^{-3}, 0.119 mm^{-3}, 0.239 mm^{-3}. From the figures, it can be known that when there is just one interference circle on CCD, the minimum measurable concentration could be calculated according to the system parameters, but with the increase of the particle concentration, the circles on CCD would overlap.

The overlap rate would decrease with the decrease of the defocusing distance, then the measurable particle concentration would increase. However, when the particle concentration continues to increase and exceeds the maximum measurable concentration, the circles of particles overlap seriously, and some can not be recognized and located successfully, which would lead to large experimental error. When this happens, changing the defocusing distance needs to be augmented with addition of the cylindrical lens to the optical set-up to compress the circular interferograms into linear interferograms [18]. The linear interferograms could be located by the corrosion matching method, then deriving the size of the interferograms. By the same identification method, the particle number can be obtained.

The simulation results of the interferograms of 10 μm, 45 μm and 90 μm particles with the two different concentrations are respectively shown in Fig. 7. In Fig. 7(a)–(c), the particle concentration is 0.0119 mm^{-3} and in Fig. 7(d)–(f), the particle concentration is 0.119 mm^{-3}. The noise added to all these images is 1% white Gaussian noise. From the Fig. 7, the fringe number is increasing with the increase of the particle size. If there are too many fringes in the interference circle, it is difficult to identify and extract the fringes. For the given system, the measurable particle size is from 10 μm to 90 μm. The measurement of other size particles can be realized by changing the system parameters.

From the Figs. 6 and 7, it can be seen that the number of the fringes is affected by the particle size, comparatively, the number of the circles is dependent on the particle concentration. Due to the particles distributed at different positions in the sampling volume, the sizes of the circles maybe not identical.

One interferogram of 45 μm particles with a concentration of $C = 0.0119\,\text{mm}^{-3}$ is simulated shown in Fig. 8(a). A 1% white Gaussian noise to the light intensity is added. Fig. 8(b) is the result of locating the interference circles by using the same algorithm in the experiment. In Fig. 8(a), the

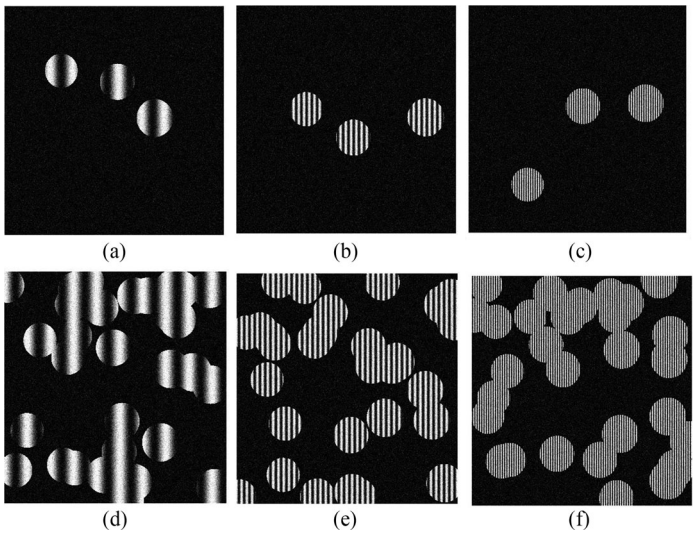

Fig. 7. Simulated interferograms of different particles under the white Gaussian noise with variance of 0.01 $C = 0.0119\,\text{mm}^{-3}$. (a) $d_p = 10\,\mu$m. (b) $d_p = 45\,\mu$m. (c) $d_p = 90\,\mu$m $C = 0.119\,\text{mm}^{-3}$. (d) $d_p = 10\,\mu$m. (e) $d_p = 45\,\mu$m. (f) $d_p = 90\,\mu$m.

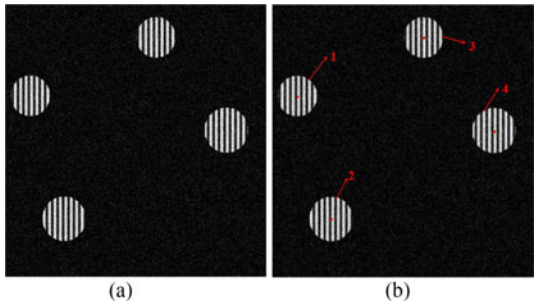

Fig. 8. (a) Particle identification in sampling volume simulated interferogram (b) result of locating interference circles.

interference circles of all four particles are recognized and located successfully. And the sizes of the interference circles are shown in the following Table 1.

From the Table 1, it can be judged that just particle 2 is not in the sampling volume. Then, the particle concentration can be calculated by $3/251.14\ \text{mm}^3 = 0.0119\ \text{mm}^{-3}$. The result has verified that the algorithm to retrieve the particle concentration works properly.

4. Experiments

4.1 Defocused IPI system

The experimental configuration of the defocused IPI is shown in the photograph of Fig. 9. The light source was a continuous semiconductor laser. Its wavelength was $\lambda = 532\,\text{nm}$ and the maximum power was 4 W. The beam expander was a $10^{\times}$ mirco-objective lens(APSF13-1AT) and the spatial filter is a 10 μm pinhole from Zolix company. The next lens is a plano-convex lens with a focal length of $f = 200$ mm (LA1979-A) and two cylindrical lenses, one plano-convex cylindrical lens of $f_1 = 500\,\text{mm}$ (LJ1144L2-A) and one plano-concave cylindrical lens of $f_2 = -20\,\text{mm}$ (LK1085L1-A) from Thorlabs company. The imaging lens is a 50 mm f/1.4 PENTAX TV lens from Nikon company. The CCD is a 14-bit digital CCD sensor from PointGrey company (GRAS-14S5M-C) with effective

TABLE 1
Processing Result of Simulated Interferogram

Particle number	X coordinate (pix)	Y coordinate (pix)	Dimension of the interference circle (pix)	Size range
1	93	325	146	[143, 146]
2	216	574	158	[146, 149]
3	539	118	155	[155, 158]
4	801	447	163	[162, 165]

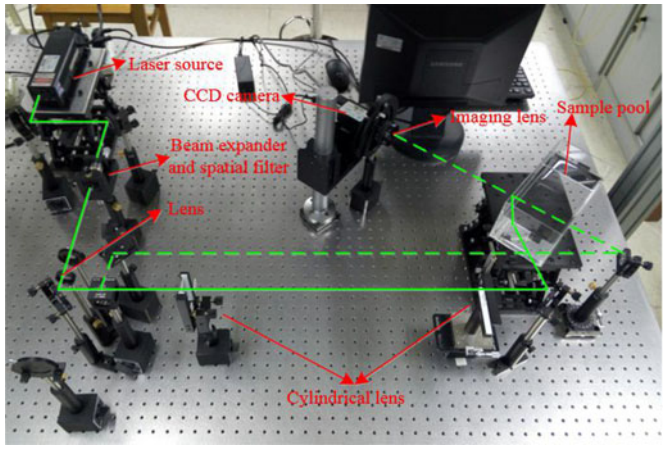

Fig. 9. Defocused IPI experimental setup.

1280 pixels $\times$ 960 pixels and a pixel size of 6.45 μm $\times$ 6.45 μm. The frame rate of the CCD is 15 fps. The laser beam becomes a collimated light with a diameter of 15 mm after passing the beam expander, spatial filter and a lens. Then the light is compressed by the cylindrical lens into a sheet beam with a thickness of $p = 0.6$ mm. The green solid lines represent the propagation path of the incident laser, and the green dashed lines mark the auxiliary light path to calibrate the height of the imaging lens and CCD when setting up the experimental system. The particles used in experiment are standard spheroids made of polystyrene divinyl-benzene latex particles, with an average, diameter of 45 μm, and a refractive index of 1.57. The concentration of the particle sample is 10^6 ml^{-1}. In the experiment, the volume of the deionized water in the sampled pool is 200 mm $\times$ 150 mm $\times$ 100 mm, within which 0.02 ml particle sample were mixed into the water. The particles were agitated for uniform distribution. The concentration of the measured particles was thus $C = 10^6 \times 0.02/(200 \times 150 \times 100) = 0.0067$ mm^{-3}. During the experiment, the sheet beam and the position of the imaging lens were fixed, the object distance was constant, and so is the collecting angle of imaging system. The image distance can be changed when changing the position of CCD by adjusting the two-dimensional translation stage. Then, the interferograms can be accepted at different defocused image plane.

4.2 Performance of Recovering Experimental Condition 1

First, the magnification of the experimental system is calibrated by locating the steel ruler at the central plane of sheet beam. The central magnification is $\beta_o = 0.20$ calculated by measuring object

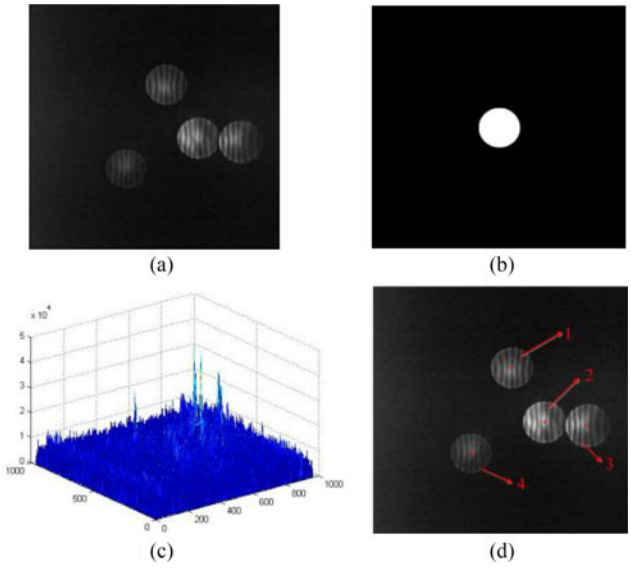

Fig. 10. Image processing. (a) Interferogram. (b) Particle mask. (c) Result of correlation calculation. (d) Result of locating interference circles.

TABLE 2
Experimental Result of 45 μm Spherical Particles

Particle number	X coordinate (pix)	Y coordinate (pix)	Dimension of the interference circle (pix)	Size range
1	521	312	156	[155, 158]
2	642	522	158	[158, 161]
3	803	536	164	[162, 165]
4	367	642	150	[151, 154]

height $y_o = 31$ mm and image height $y_o' = 6.192$ mm. The object distance is $u_o = 300.4$ mm, the image distance is $v_o = 60$ mm and the backward defocusing distance is 1.68 mm.

An example of image processing result is shown in Fig. 10. Fig. 9(a) shows the interferogram of the spherical particles in particle field. The diameter of the measured particle is 45 μm. The image is cut from the central position 960 pixels $\times$ 960 pixels on CCD. Fig. 10(b) is the image of particle mask. Fig. 10(c) is the correlation calculation result of the particle mask with the interferogram. In Fig. 10(c), four peaks of the correlation calculation can be obviously observed and their positions express the central positions of the interference circles. The size of the particle mask with maximum correlation value is regarded as the size of the interference circle. Fig. 10(d) is the result of locating interference circles, in which the red points are used to label the central positions. The interference circles of all four particles are recognized and located successfully. And the central coordinates and diameters of the interference circles are shown in the following Table 1.

From the Table 2, we can know that the diameter of the number 4 circle is 150 pixels, and at the position (367, 642) on CCD the size range is [151, 154]. Then, we can judge that this particle is not in the sampling volume. Therefore, it should be ignored when counting the particle number in sampling volume and calculating the particle concentration.

In experiment, 53 pictures have been collected. The experimental results of the circle size with the position on CCD are shown as Fig. 11.

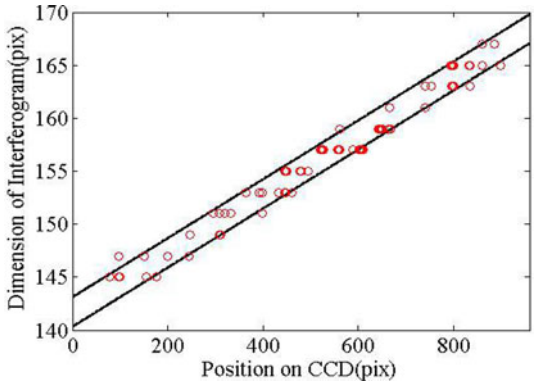

Fig. 11. Experimental result of 45 μm spherical particles.

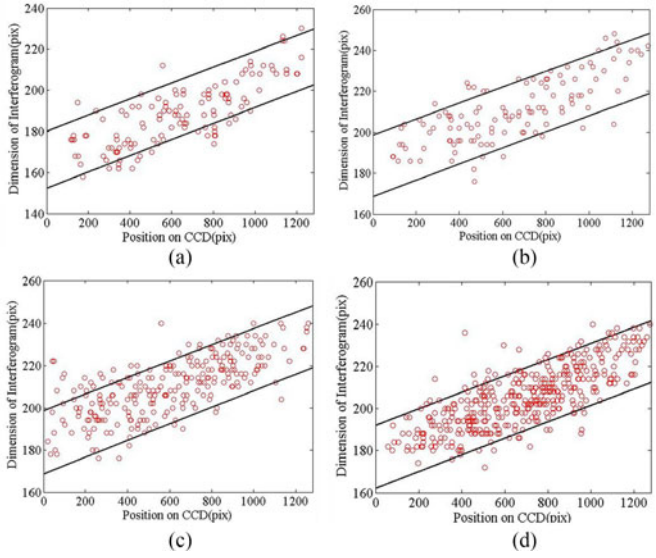

Fig. 12. Experimental results of different particles. (a) $d_p = 10\,\mu$m, $C = 0.05\,\text{mm}^{-3}$, $g = 5.84\,$mm. (b) $d_p = 21.3\,\mu$m, $C = 0.045\,\text{mm}^{-3}$, $g = 6.34\,$mm. (c) $d_p = 21.3\,\mu$m, $C = 0.09\,\text{mm}^{-3}$, $g = 6.34\,$mm. (d) $d_p = 10$ and $21.3\,\mu$m, $C = 0.14\,\text{mm}^{-3}$, $g = 6.14\,$mm.

In Fig. 11, the range between the two black lines represents the size range of the interference circle formed by the particles in the effective area illuminated by the sheet beam theoretically. Also, the red circles express the experimental results. 93 particles are recognized and located successfully. 80 particles are in the corresponding size range and other 13 particles are not. The sampling volume is 251.14 mm^3 calculated according to (1)–(9), so the concentration of measured field is (80/53)/251.14 = 0.006 mm^{-3}. The relative error is (0.0067–0.006)/0.0067 = 10.4%.

4.3 Performances of Recovering Experimental Condition 2

The system parameters have been changed and other experiments with particles of different sizes have been done. First, the central magnification is 0.688. The object distance is $u_o = 122.67\,$mm, the image distance is $v_o = 84.4\,$mm. The thickness of the sheet beam is $p = 1.6$ mm. We put different particle samples into the deionized water respectively. For every measurement, 36 images are recorded at different times and the defocusing distance are also different. The interferograms of particles are cut from the different positions on CCD. The experimental results are shown as Fig. 12.

TABLE 3
Experimental Result of Spherical Particles

Particle diameter (μm)	Particle concentration (mm^{-3})	Sampling volume (mm^3)	Experimental results (mm^{-3})	Relative error
45	0.0067	251.14	0.006	10.4%
10	0.05	73.74	0.0448	10.4%
21.3	0.045	72.92	0.0411	8.7%
21.3	0.09	72.92	0.0852	5.3%
10 + 21.3	0.14	73.25	0.138	1.4%

In Fig. 12(a), 142 particles are recognized and located successfully, and 119 particles are in the corresponding size range. In Fig. 12(b), 108 of all 130 particles are in the corresponding size range. In Fig. 12(c), 224 of all 256 particles are in the corresponding size range. In Fig. 12(d), 366 of all 414 particles are in the corresponding size range.

Table 3 shows the experimental results of particles with different sizes and concentrations. According to the data in Table 3, it can be deduced that our method to identify the particle in sampling volume is feasible and can provide important information for concentration calculation.

5. Discussions

From (1)–(9), it can be known that the sample volume of defocused IPI is related with focal length f, central magnification β_o, thickness of sheet beam p and defocusing distance g. So, to increase the sampling volume, the following steps could be used.

a) Use an imaging lens that has a longer focal length.
b) Apply smaller magnification to the central area of the sheet beam.
c) Increase the thickness dimension of the sheet beam.
d) Reduce the backward defocusing distance.

When identifying the particle in the sampling volume, after obtaining the defocused interferograms, it is necessary to confirm the central coordinates of the interference circle on CCD. Next, according to the coordinate on CCD, the experimental size Φ and theoretical size range $[\Phi_{pix2}, \Phi_{pix1}]$ can be calculated and compared. Thus, the particle identification in sampling volume can be realized.

For measuring the particle field with high concentration, the problem of interferograms' overlap can be solved effectively by changing the defocusing distance or adding cylindrical lens to the optical system, but generally, the interference circles of particles can be full of entire image but not overlap to ensure the measurement accuracy. For the experimental set-up in Fig. 7, the range of measurable particle concentration is from 0.004 mm^{-3} to 0.203 mm^{-3}.

In experiment, a number of particles are recognized, but not all particles are in the sampling volume. There are several reasons. The particles are dissolved in deionized water in a sample pool, and the light would refract at the air-water interface. The thickness and divergence angle of the sheet beam might be affected to make the measured volume bigger than the theoretically calculating volume. Another reason of error is the presence of stray light. The scattered light consisting of reflected light and refracted light may be reflected and refracted again by other particles. Therefore, the particles not in sampling volume may be illuminated and recorded on CCD. But in actual particle measurement, the incident light wouldn't be affected by the sample pool so the accuracy of measuring result would be better.

In our experiment, the calculation error of the particle concentration is related with the sampling volume and the particle number. The measurement error of the thickness of the sheet beam and the scattering angle may cause the calculation error of the sampling volume. And the experimental results of particle concentrations are always smaller than the practical values. These unferestimations may have been caused by the experimental conditions whereby the particles were put into the sample pool and some particles were attached to the wall. This would lead to the smaller particle number in sampling volume. This would finally result in the smaller particle concentration, but when measuring actual particle field, the result would not be affected by sample pool, and the measurement accuracy can be improved.

6. Conclusion

In conclusion, we have demonstrated a method for determining the sampling volume of defocused IPI and identifying whether particles are in this region. Sampling volume is calculated based on the geometrical optics. It is related with the parameters of focal length, central magnification, thickness of the sheet beam and defocusing distance. When the thickness of the sheet beam laser is fixed, the size range $[\Phi_{pix2}, \Phi_{pix1}]$ of the interference circle of every imaging position on CCD can be derived theoretically. According to the size of the interference circle collected in experiment, whether the particle is in the sampling volume or not can be confirmed. According to the analyses, sampling volume and particle number can be obtained, thus providing information to calculate the particle concentration. The experimental results and theoretical analyses are in good agreement. This method has wide application in various particle fields.

Acknowledgment

The authors would like to thank the anonymous reviewers, as well as Dr. D. Piao of Oklahoma State University for helping improve the technical content and presentation of this manuscript.

References

[1] G. Konig, K. Anders, and A. Frohn, "A new light-scattering technique to measure the diameter of periodically generated moving droplets," *J. Aerosol. Sci.*, vol. 17, no. 2, pp. 157–167, 1986.
[2] S. M. Skippon and Y. Tagaki, "ILIDS measurements of the evaporation of fuel droplets during the intake and compression strokes in a firing lean burn engine," *SAE Trans.*, vol. 105, no. 3, pp. 1111–1126, Feb. 1996.
[3] C. M. Rousselle and O. Pajot, "Droplet sizing by Mie scattering interferometry in a spark ignition engine," *Part. Part. Syst. Characterization*, vol. 16, no. 4, pp. 160–168, Oct. 1999.
[4] N. Damaschke, H. Nobach, and C. Tropea, "Optical limits of particle concentration for multi-dimensional particle sizing techniques in fluid mechanics," *Exp. Fluids*, vol. 32, no. 2, pp. 143–152, Oct. 2001.
[5] H. E. Albrecht *et al.*, *Laser Doppler and Phase Doppler Measurement Techniques*. Heidelberg, Germany: Springer, 2003.
[6] Y. Niwa *et al.*, "Bubble sizing by interferometric laser imaging," in *Proc. 10th Int. Symp. Appl. Laser Techn. Fluid Mech.*, Lisbon, Portugal, pp. 1–11, 2000.
[7] Y. Zama, M. Kawahashi and H. Hirahara, "Simultaneous measurement method of size and 3D velocity components of droplets in a spray field illuminated with a thin laser-light sheet," *Meas. Sci. Technol.*, vol. 16, no. 10, pp. 1977–1986, Oct. 2005.
[8] A. Querel *et al.*, "Real-time global interferometric laser imaging for the droplet sizing (ILIDS) algorithm for airborne research," *Meas. Sci. Technol.*, vol. 21, no. 1, Dec. 2009, Art. no. 015306.
[9] H. Shen, S. Coëtmellec, and M. Brunel, "Cylindrical interferometric out-of-focus imaging for the analysis of droplets in a volume," *Opt. Lett.*, vol. 37, no. 19, pp. 3945–3947, Oct. 2012.
[10] M. Brunel *et al.*, "Determination of the size of irregular particles using interferometric out-of-focus imaging," *Int. J. Opt.*, vol. 2014, no. 2014, Jan. 2014, Art. no. 143904.
[11] P. G. Carrascal, S. G. Ruiz, and J. van Beeck, "Irregular particle sizing using speckle pattern for continuous wave laser applications," *Exp. Fluids*, vol. 55, no. 1851, pp. 1–10, Oct. 2014.
[12] M. Maeda, T. Kawaguchi, and K. Hishida, "Novel interferometric measurement of size and velocity distributions of spherical particles in fluid flows," *Meas. Sci. Technol.*, vol. 11, no. 12, pp. L13–L18, 2000.
[13] N. Damaschke, H. Nobach, and C. Tropea, "Optical limits of particle concentration for multi-dimensional particle sizing techniques in fluid mechanics," *Exp. Fluids*, vol. 32, no. 2, pp. 148–152, 2002.
[14] H. B. Evans *et al.*, "Measuring droplet size distributions from overlapping interferometric particle images," *Rev. Sci. Instrum.*, vol. 86, no. 2, Feb. 2015, Art. no. 023709.

[15] Y. Wang and R. K. Wang, "Measurement of particle concentration in flow by statistical analyses of optical coherence tomography signals," *Opt. Lett.*, vol. 36, no. 1, pp. 2143–2145, Jun. 2011.
[16] S. Buaprathooma *et al.*, "High concentration measurement of mixed particle suspensions using simple multi-angle light scattering system," *Proc. SPIE*, vol. 8439, 2012, Art. no. 843923.
[17] H. Zhang *et al.*, "Theoretical analysis and experimental validation of sampling volume in tilted imaging system," *IEEE Photon. J.*, vol. 7, no. 6, Dec. 2015, Art. no. 6901412.
[18] Q. X. Wang *et al.*, "Linear interferometric image processing for analysis of a particle in a volume," *J. Opt.*, vol. 16, no. 4, Mar. 2014, Art. no. 045703.